The effects of co-addition of La and Nd on microstructures and mechanical properties of squeeze-cast Mg-Al-Zn-La-Nd alloys

P. Cui[1], Z. Ji[1], M. Hu[1]*, H. Xu[1], X. Zhang[1], T. Zhang[2]

[1] *School of Materials Science and Engineering, Harbin University of Science and Technology, Harbin 150080, P. R. China*
[2] *Faculty of Science and Engineering, Department of Electrical and Electronic Engineering, University of Nottingham, Ningbo 315100, P. R. China*

Abstract

The effects of co-addition of La and Nd on microstructures and mechanical properties of squeeze-cast Mg-Al-Zn-La-Nd alloys were investigated. Six squeeze-cast Mg-Al-Zn-La-Nd alloys with different La/Nd ratios were prepared. Microstructures, Vickers hardness, and compression properties (at room temperature and high temperature) were investigated. The results reveal that the La/Nd ratio has a significant influence on the microstructure and mechanical properties. The microstructure, $Mg_{17}Al_{12}$ area fraction, Vickers hardness, and compression properties of alloys with different La/Nd ratios are different. When the La/Nd ratio is 2/3, the alloy has fine grains, less $Mg_{17}Al_{12}$ phase content, and excellent mechanical properties. The present research indicates that adding dual REs with appropriate La/Nd ratio to Mg-Al-Zn alloy can effectively improve its performance.

K e y   w o r d s: AZ91, rare earth, microstructure, mechanical properties, squeeze-cast

1. Introduction

AZ91 alloy, which mainly contains 9 wt.% Al and 0.8 wt.% Zn, is increasingly used in vehicle components due to their excellent die castability and satisfactory corrosion resistance [1]. However, $Mg_{17}Al_{12}$ leads to the deterioration in mechanical properties at 473 K, which limits the application of AZ91 on automobile powertrain components [2]. Many researchers focus on improving alloy structure, reducing internal defects, and improving alloy properties through RE alloying and squeeze casting process [3, 4]. REs do not form Mg-RE or Mg-RE-Al phases in Mg-Al alloys because of the difference in electronegativity between the elements [5, 6]. Pettersen et al. [7] reported that REs used have quite similar properties and are found to combine with Al to form the $Al_{11}RE_3$ phase (and $Al_{10}RE_2Mn_7$) in Mg-Al alloys. However, Powell et al. [8] were the first to think that the formation of $Al_{11}RE_3$ and Al_2RE is sensitive to rare earth individuals. They also reported that La preferentially favors the formation of the $Al_{11}RE_3$ phase, while Nd favors the Al_2RE phase. Those phases with a low La : Nd ratio (less than 0.7) are Al_2RE, and when La : Nd ratio is high, $Al_{11}RE_3$ is formed. Zou et al. [9] proposed that $Al_{11}Nd_3$ is easily formed in the high Nd concentration area because the proeutectic polygon Al_2Nd promotes nucleation to accelerate the peritectic formation of $Al_{11}Nd_3$. Zhang et al. [10] reported that the decomposition energy of the $Al_{11}RE_3$ phase was calculated by first-principles and super-soft pseudopotentials. The conclusion is that the decomposition energy of $Al_{11}La_3$ is the highest, and the thermal stability of $Al_{11}RE_3$ is sensitive to rare earth individuals. The individual differences of rare earth are also reflected in the solubility in Mg alloys (the solubility of La is 0.79 wt.% and Nd is 3.60 wt.% [11]). In the study by the author [12] on the microstructure and properties of AZ91-xRE ($x = 0, 1, 2, 3$), the alloy containing 2 wt.% RE exhibits the highest properties (hardness, fluidity, tensile strength, etc.). Similar studies by Bayani et al. [13] also revealed that the same amount of RE addition could significantly improve the thermal properties of AZ91.

The squeeze casting process, also called "liquid metal forging," is a metal process that combines

*Corresponding author: e-mail address: humaoliang@hrbust.edu.cn

Table 1. Chemical composition of the investigated Mg-Al-Zn-La-Nd alloys

Alloys code		La : Nd	Analyzed composition (wt.%)						
			La	Nd	Al	Zn	Mn	Si	Mg
S1	Squeeze-cast	0 : 0	0.00	0.00	8.66	0.73	0.16	0.051	Bal.
S2	Squeeze-cast	1 : 3	0.51	1.48	8.48	0.75	0.17	0.053	Bal.
S3	Squeeze-cast	2 : 3	0.78	1.20	8.67	0.73	0.17	0.059	Bal.
S4	Squeeze-cast	1 : 1	0.99	1.01	8.57	0.72	0.18	0.058	Bal.
S5	Squeeze-cast	3 : 2	1.21	0.77	8.61	0.72	0.17	0.053	Bal.
S6	Squeeze-cast	3 : 1	1.49	0.51	8.56	0.74	0.17	0.054	Bal.

casting and forging to reduce defects where molten metal is solidified under an applied pressure [14]. The squeeze-casting molding process that combines casting and forging helps magnesium alloy parts be better used in automobiles [15]. Lee et al. [16] reported that the grain sizes of the squeeze-cast AZ91-X alloys with added alloying elements (Y, Sr, and Nd) are finer than those of the squeeze-cast AZ91 alloy. Zhang et al. [17] reported that the squeeze casting process suppressed the negative effect of adding Ca to the AZ91 alloy on the mechanical properties. The improvement of mechanical properties is attributed to the refinement of the microstructure, the modification of the second phase, and the reduction of defects in squeeze casting.

Since the Al-RE phase is sensitive to rare earth individuals and plays a very important role in affecting the mechanical properties of Mg-Al-based alloys, further investigation is necessary and valuable for future alloy design. This work studied the influence of the La/Nd ratio on the microstructure of alloys and the morphology of the secondary phase. La/Nd ratio (1/3, 2/3, 1/1, 3/2, and 3/1) is selected as a variable, and the total amount (2 wt.%) of La and Nd is used as a constant. Vickers hardness and compressive properties are examined to understand better the mechanism of the La/Nd ratio on the properties of squeeze-cast Mg-Al-Zn-La-Nd alloys. The work aimed to obtain the most suitable La/Nd ratio in the RE alloying of Mg-Al-Zn-La-Nd alloys to make its thermal properties excellent.

2. Experimental details

Mg-Al-Zn-La-Nd alloys were prepared by melting the ingots of AZ91D and master alloys Mg--15wt.%La, Mg-20wt.%Nd in a furnace at 1023 K under the protection of CO_2 and SF_6 (99 : 1). The melt was held for 20 min to dissolve completely and then cooled to 993 K. In the squeeze casting process, the melt was transferred into the filling chamber and injected into the mold by an SCH-350A model squeeze casting machine. The applied pressure was

120 MPa, and the injection speed was 0.15 m s^{-1}. After solidification, the chemical composition (listed in Table 1) of Mg-Al-Zn-La-Nd alloys was tested by ICP-AES (Inductively Coupled Plasma-Atomic Emission Spectroscopy). Microstructural observations were performed using a metallographic optical microscope (OM, Leica LCMS301) and scanning electron microscope (SEM, FEI QUANTA-200) equipped with dispersive X-ray spectroscope (EDX, OXFORD INCA X-ACT). For microstructural observations, the squeeze-cast specimens ($15 \times 8 \times 8$ mm^3) were cut from each alloy and etched with 4 % nital. The mean grain diameter analysis was conducted using OM images (1000×750 μm^2) with Image-pro. The phase analyses were performed with an X-ray diffractometer (XRD, X' Pert Pro MPD/Cu Kα). The scanning angle (2θ) was from 10° to 100° and the measurements operated at 40 kV and 40 mA. The transmission electron microscope (TEM, HRTEM JEM-2100) at 200 kV was employed to conduct the phase analysis. For the TEM analysis, ø 1.5 mm discs were cut from 40 μm-thinned samples. Vickers hardness tests were conducted using Vickers Optical Hardness Tester (HBRVU-187.5) at a load of 500 g with a dwelling time of 15 s for all samples ($8 \times 8 \times 5$ mm^3). The average hardness ratio of each alloy was calculated from five tested ratios. The fabricated cylindrical bars (ø 10×25 mm^2) for the compression tests were machined from each alloy. The compression tests were performed at room temperature (293 K) and high temperature (423 K) by using a WDW-200 electronic universal testing machine at a rate of 1 mm min^{-1}.

3. Results and discussion

3.1. Microstructures of squeeze-cast Mg-Al-Zn-La-Nd alloys

Figure 1 shows the optical micrograph with the corresponding average grain diameter of squeeze-cast alloys: S1–S6. It reveals that all six alloys are mainly composed of approximately equiaxed α-Mg grains and plenty of interdendritic secondary phases. The mea-
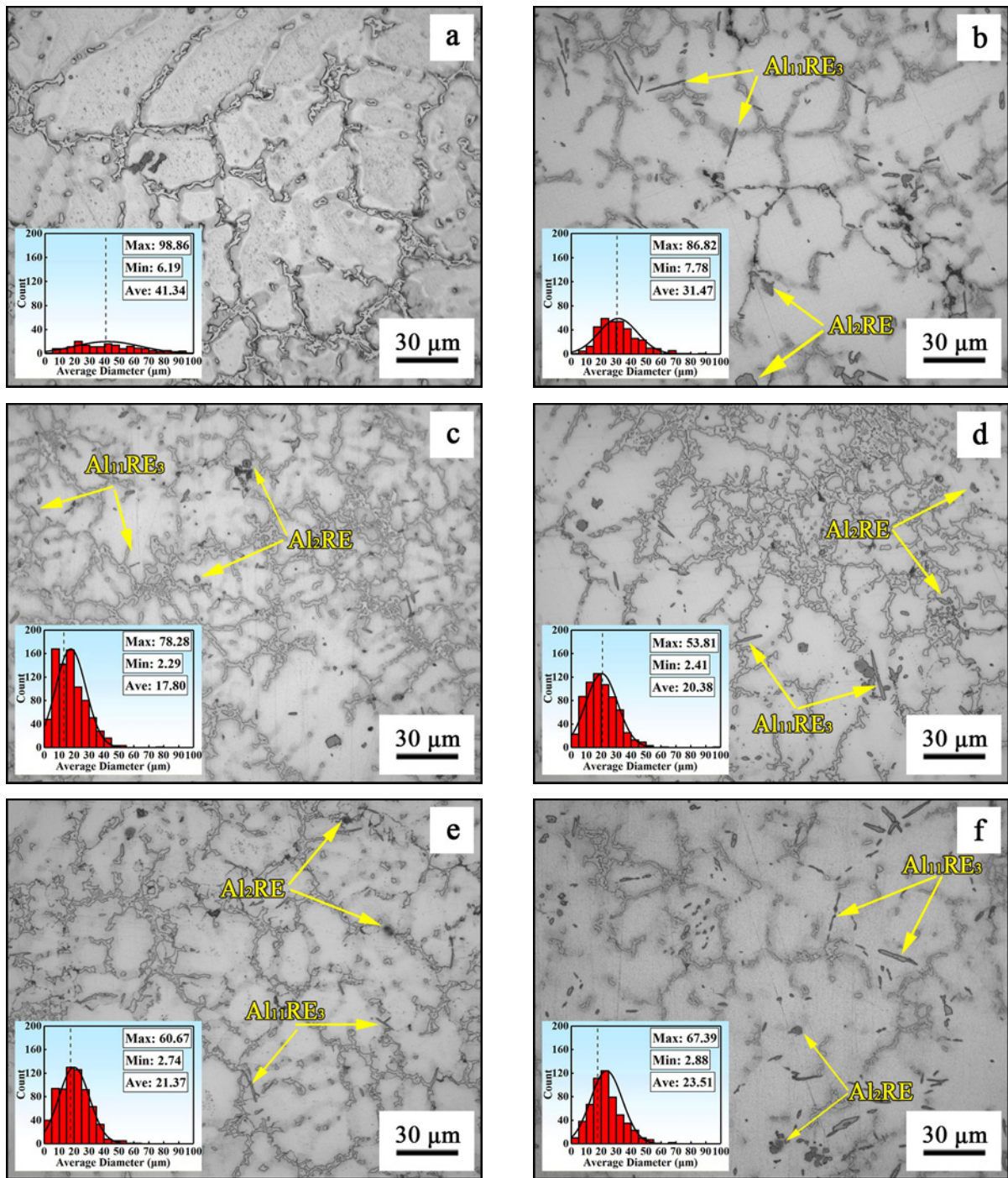
Fig. 1. Microstructures of squeeze-cast alloys with corresponding average grain diameter distribution: (a) S1; (b) S2; (c) S3; (d) S4; (e) S5; (f) S6.

sured average grain size of squeeze-cast alloys decreases from 41.34 to 17.80 μm as the La/Nd ratio increases from 0/0 to 2/3. When the La/Nd ratio increases from 2/3 to 3/2, the average grain size increases slightly to 23.51 μm. Adding REs to the squeeze-cast alloys, the grains in the alloys are refined significantly, and the $Mg_{17}Al_{12}$ phases around grain boundaries are significantly modified. Refs. [18,

19] also reported the grain refinement effect of REs on AZ91. The values of electronegativity of Mg, Al, La, and Nd are 1.31, 1.61, 1.10, and 1.14, respectively [20, 21]. It is indicated that thermal stable $Al_{11}RE_3$ and Al_2RE are easier to form than other intermetallic compounds [5]. According to [9], the Al-RE phase $(Al_{11}RE_3)$ formed during the grow-up period of the α-Mg nucleus. The Al-RE phase existing in the in-
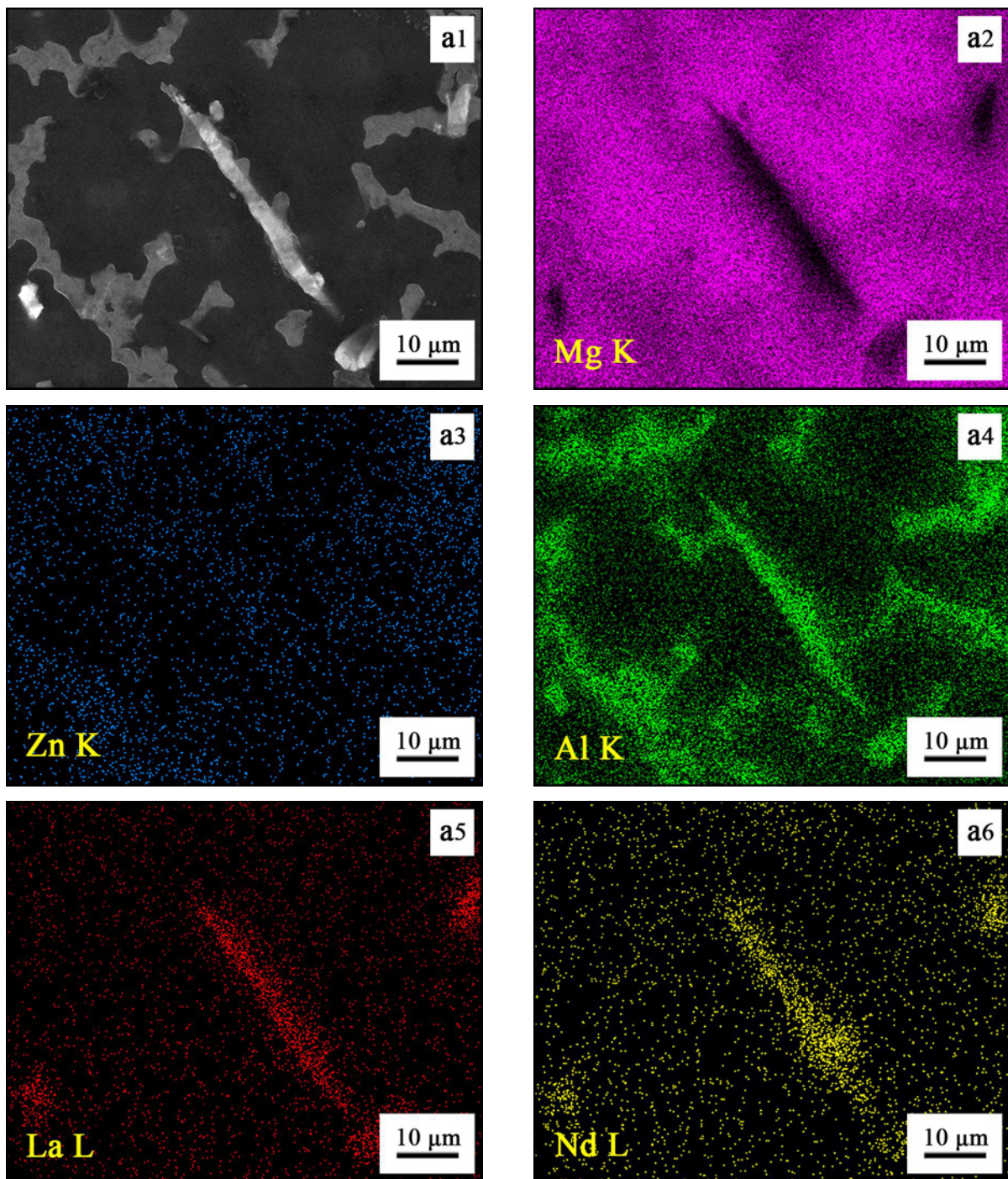
Fig. 2a1–6. EDS analyses of squeeze-cast Mg-Al-Zn-La-Nd alloy: (a1) SEM image of Mg-Al-Zn-La-Nd alloy; (a2) Mg K; (a3) Zn K; (a4) Al K; (a5) La L; (a6) Nd L.

ner and outer regions of grain hinders grain growth and refines grain size. As shown in Fig. 1, two types of Al-RE phases (marked by arrow) exist in the microstructures of squeeze-cast Mg-Al-Zn-La-Nd alloys, i.e., needle-shaped $Al_{11}RE_3$ being the dominant one and the polygonal Al_2RE. Because of the thermal stability of Al-RE, Al-RE plays a key role in improving the room temperature (RT) and high temperature

(HT) properties of the squeeze-cast Mg-Al-Zn-La-Nd alloys. The measured β-$Mg_{17}Al_{12}$ area frictions are 29.36, 13.05, 5.76, 4.31, 9.51, and 11.96 % for squeeze-cast alloys (S1–S6) indicating that the addition of REs (La and Nd) significantly suppresses the precipitation of β-$Mg_{17}Al_{12}$. As the La/Nd ratio increases, the area friction of β-$Mg_{17}Al_{12}$ decreases first and then increases. The alloy with the smallest β-$Mg_{17}Al_{12}$ area
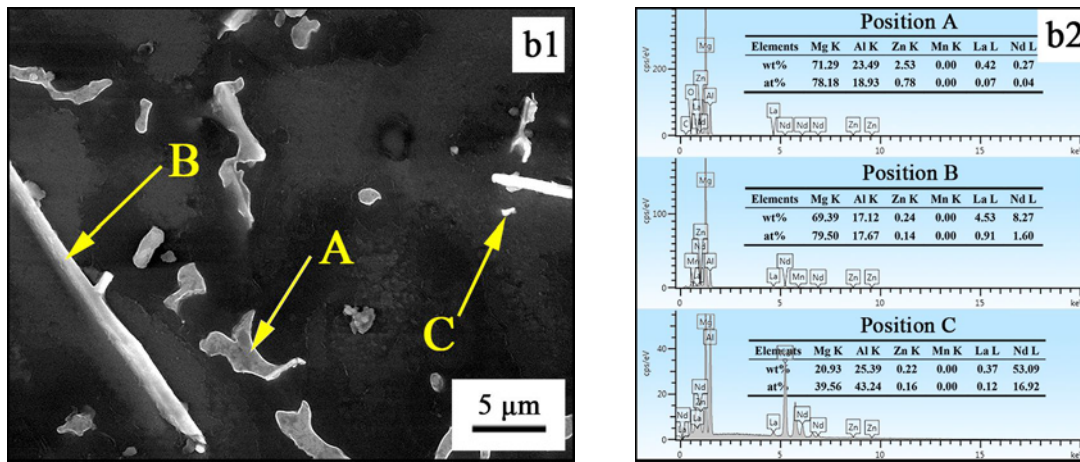
Fig. 2b1, b2. EDS analyses of squeeze-cast Mg-Al-Zn-La-Nd alloy: (b1) enlarged SEM image of Mg-Al-Zn-La-Nd alloy; (b2) EDS results of position A, B, and C.
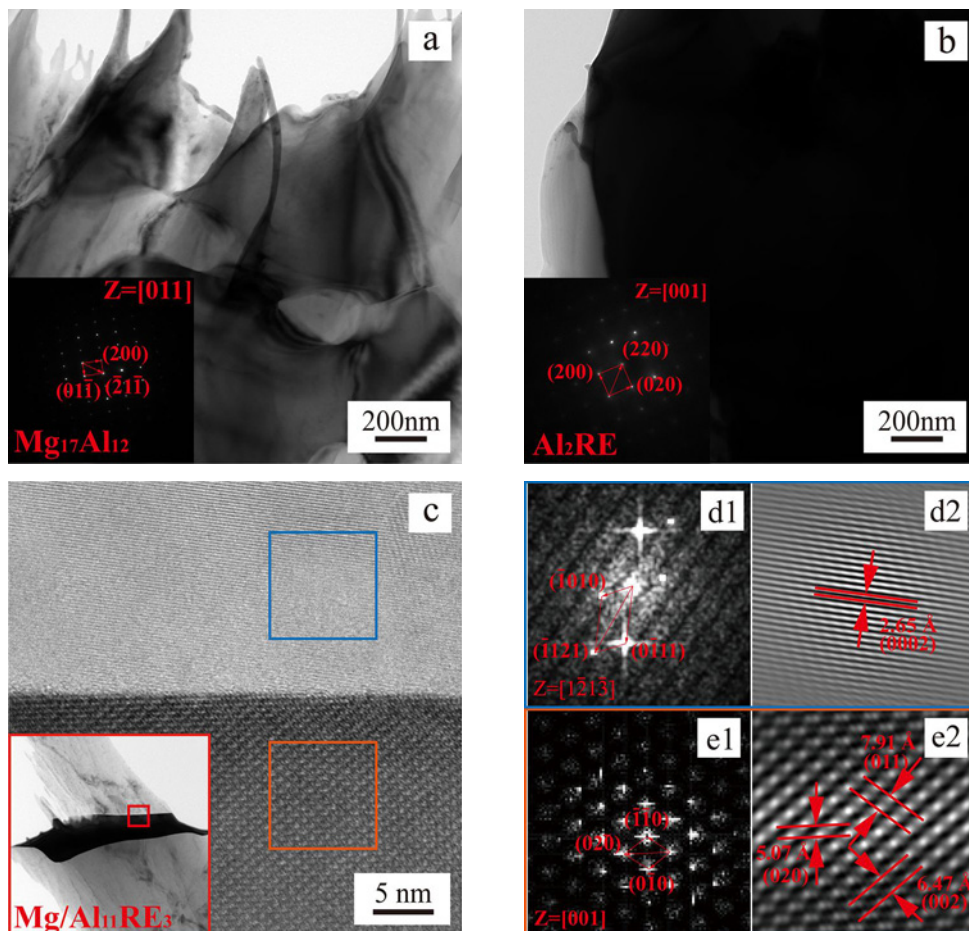
Fig. 3. Bright field (BF) images and selected area electron diffraction (SAED) patterns: (a) $Mg_{17}Al_{12}$ and (b) Al_2RE; (c) BF images and HRTEM patterns of $Al_{11}RE_3$; (d1) FFT pattern of Mg and (d2) Fourier-filtered image of (d1); (e1) FFT pattern of $Al_{11}RE_3$ and (e2) Fourier-filtered image of (e1).

fraction is the alloy with a La/Nd ratio of 1/1.

Figure 2a shows the EDS elemental mappings of squeeze-cast Mg-Al-Zn-La-Nd alloy with REs addition. Al, La, and Nd elements are concentrated in the

locations of the white needle-shaped phase and white granular phase. Mg and Al elements are concentrated in the dark gray coarse bulk phase. Besides, the area where the Al element concentrates in each phase is
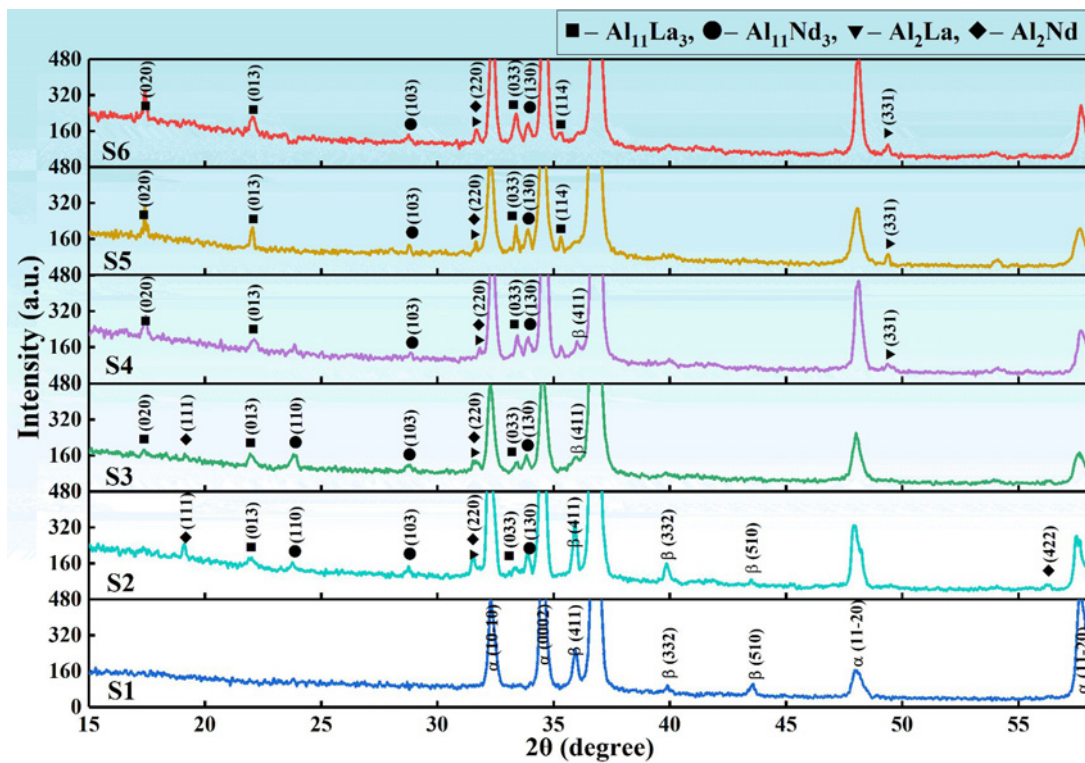
Fig. 4. XRD analysis of squeeze-cast alloys: (a) scanning angle from 16.9° to 35°; (b) scanning angle from 34.6° to 58.1°.

slightly larger than that for other elements (La and Nd), which indicates that the Al element is easy to concentrate and distribute around these phases. The EDS analyses of bulk phase (point A), needle-shaped phase (point B), and granular phase (point C) are shown in Fig. 2b. Analyses by TEM (Fig. 3) and EDS reveal that the observed bulk phase is $Mg_{17}Al_{12}$ (body-centered cubic structure, $a = 1.06$ nm), the granular phase is Al_2RE (face-centered cubic structure, $a = 0.82$ nm), and the needle-shaped phase is $Al_{11}RE_3$ (body-centered orthorhombic structure, $a = 0.43$ nm, $b = 1.29$ nm, $c = 1.01$ nm).

Figure 3c shows the TEM bright field (BF) image and high-resolution TEM (HRTEM) image of $Mg/Al_{11}RE_3$ interface. Fast Fourier transformation (FFT) analysis of two squared area marked in Fig. 3c is shown in Figs. 3d1,e1, respectively. One-dimensional inverse-FFT images in Figs. 3d2,e2 reveal the secondary phase $Al_{11}RE_3$ tends to grow with its (020) planes parallel to that of the (0002) of the α-Mg matrix. These observations agree with the report [20]. The majority of $Al_{11}RE_3$ phases are formed on the basal plane (0002) of the matrix, which is useful in blocking the movement of dislocations in the basal plane.

Figure 4 shows the XRD spectra from squeeze--cast alloys: S1–S6. The phase identification was carried out by comparing the position and intensity of the diffraction peak in the spectrum with the data in ICDD PDF4-2009. The results show that the main

phase components of the squeeze casting Mg-Al-Zn--La-Nd alloy are $Mg_{17}Al_{12}$, $Al_{11}La_3$, $Al_{11}Nd_3$, Al_2La, and Al_2Nd. With increasing La/Nd ratio, the intensity of the $Al_{11}La_3$ (crystal plane of (020)) and Al_2La (crystal plane of (331)) increased while the intensity of $Al_{11}Nd_3$ (crystal plane of (110)) and Al_2Nd (crystal plane of (111)) decreased. It is worth mentioning that the changes in the two characteristic peaks with scanning angles of 33.47° and 33.92° are consistent with the changes in the content of rare earth elements. With the increase of La/Nd ratio, the peak corresponding to (033) the plane reflection of $Al_{11}La_3$ increases, and the peak corresponding to (130) the plane reflection of $Al_{11}Nd_3$ decreases. Besides, the peak of Al_2Nd at 56.26° almost disappeared when La/Nd ratio was greater than 1/1, while the peak of $Al_{11}La_3$ at 35.40° and Al_2La at 48.67° emerged. Interestingly, the $Mg_{17}Al_{12}$ peak of (411) the plane at 36.19° and (332) plane at 40.22° increased when La/Nd ratio was 1/3. As the La/Nd ratio increased from 1/3 to 3/1, these two peaks of $Mg_{17}Al_{12}$ were significantly weakened. It reveals that the content of $Mg_{17}Al_{12}$ is greatly reduced because of the addition of RE, reducing the Al level in the Mg matrix and suppressing the precipitation of $Mg_{17}Al_{12}$ [22].

3.2. Thermodynamic analysis

The addition of RE (La and Nd) to AZ91 alloy leads to the formation of $Al_{11}RE_3$ and Al_2RE with-

out any formation of Mg-RE or Mg-Al-RE phases due to the electronegative difference between Al and RE is greater than that between Mg and RE [7, 23]. The Miedema model can be used to perform thermodynamic calculations on the results mentioned above [24, 25]. The enthalpy of formation ΔH can be calculated using the following expressions:

$$\Delta H = c_A^s c_B^s \frac{2 \left(c_A V_A^{2/3} + c_B V_B^{2/3} \right)}{(n_{ws}^A)^{-1/3} + (n_{ws}^B)^{-1/3}} \cdot \left[Q \left(\Delta n_{ws}^{1/3} \right)^2 - P \left(\Delta \varphi^* \right)^2 \right], \qquad (1)$$

$$\Delta H = c_A^s c_B^s \left[1 + \lambda \left(c_A^s c_B^s \right)^2 \right] \frac{2P \left(c_A V_A^{2/3} + c_B V_B^{2/3} \right)}{(n_{ws}^A)^{-1/3} + (n_{ws}^B)^{-1/3}} \cdot \left[\frac{Q}{P} \left(\Delta n_{ws}^{1/3} \right)^2 - P \left(\Delta \varphi^* \right)^2 - \frac{R}{P} \right], \qquad (2)$$

where c_A and c_B are atomic concentrations of metals A and B, V_A and V_B are molar volumes of metals A and B, c_A^s and c_B^s are surface concentrations of metals A and B; other experimental data can be obtained from [24]. Equation (1) applies to two non-transition metals (Mg and Al), Eq. (2) applies to transition metal with non-transition metal (RE and Al). The enthalpy of formation is related to the order of alloy formation. The smaller the enthalpy, the easier it is to form, and the more stable the intermetallic phase will be. The main phases in Mg-Al-Zn-La-Nd alloys are $Mg_{17}Al_{12}$, $Al_{11}La_3$, Al_2La, $Al_{11}Nd_3$, and Al_2Nd. The ratio ΔH calculated from the above formula is –11, –38, –50, –41, and –53.6 kJ mol^{-1}. The results reveal that the formation enthalpy of the Al-RE is much smaller than that of $Mg_{17}Al_{12}$, so Al-RE is easier to form. The difference in enthalpy of formation between Al-RE phases is small and formed during the grow-up of α-Mg [9]. In addition, the solubility of Nd is 3.60 wt.%, and the solubility of La is 0.79 wt.%. The solid solubility of Nd is much greater than that of La. At a large La/Nd ratio, more La elements tend to form needle-shaped $Al_{11}RE_3$ in the alloy. On the contrary, there are more Nd elements that tend to form polygonal Al_2RE in the alloy. In alloys with different La/Nd ratios, the contents of $Al_{11}RE_3$ and Al_2RE are different.

3.3. Effect of REs on the microstructure evolution

Figures 5a,b show the magnified views of intermetallic compounds in Mg-Al-Zn alloy without REs added and Mg-Al-Zn-La-Nd alloy with REs added, respectively. It is observed from Fig. 5b that the massive
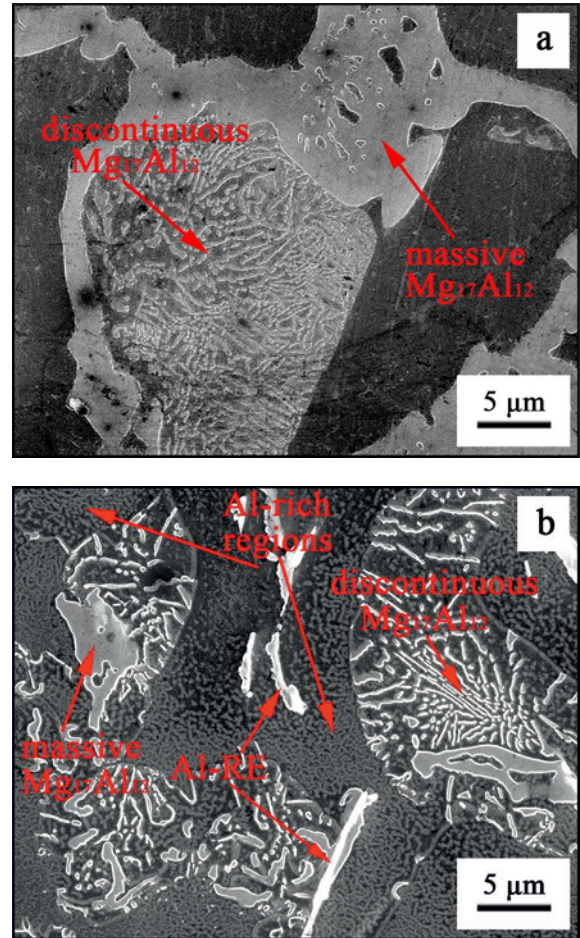
Fig. 5. Magnified views of intermetallic compounds in: (a) the Mg-Al-Zn alloy and (b) the Mg-Al-Zn-La-Nd alloy.

$Mg_{17}Al_{12}$ (isolated lath-shaped $Mg_{17}Al_{12}$) becomes semi-continuous or discontinuous precipitation after adding REs. At the same time, the content of the discontinuous precipitation (dense lamellar $Mg_{17}Al_{12}$) is significantly reduced. Amir Esgandari et al. [3] reported that RE led to the complete suppression of $Mg_{17}Al_{12}$. During the solidification, REs create the constitution undercooling at the solid/liquid interface, which contributes to the nucleation of α-Mg. REs and Al are enriched in residual liquid, so REs consume Al elements to form Al_xRE_y at the grain boundary and inhibit the growth of $Mg_{17}Al_{12}$. Consequently, the growth of grains is restricted, and grains are refined. According to the Hall-Petch relationship, fine grains can significantly improve mechanical properties [26].

3.4. Mechanical properties of squeeze-cast Mg-Al-Zn-La-Nd alloys

Table 2 shows the Vickers hardness and compressive properties of squeeze-cast alloys: S1–S6. The Vickers hardness first increases rapidly as La/Nd ratio rises

T a b l e 2. Mechanical properties of squeeze-cast alloys

Alloys code	Vickers hardness, HV	Compressive properties (MPa)	
		Room temperature (293 K)	High temperature (423 K)
S1	63.71 ± 4.03	300.50 ± 8.84	283.98 ± 9.65
S2	70.14 ± 3.16	341.35 ± 11.71	312.18 ± 7.62
S3	82.15 ± 3.35	361.38 ± 13.78	346.55 ± 12.11
S4	75.98 ± 2.78	370.19 ± 14.21	327.14 ± 12.11
S5	70.01 ± 3.72	356.35 ± 7.82	311.67 ± 9.73
S6	65.88 ± 4.01	351.16 ± 9.24	302.31 ± 7.93

up and then decreases. When La/Nd ratio is 2/3, Vickers hardness reaches the peak ratio (S3). Besides, increasing the La/Nd ratio from 0/0 to 1/1 results in an increase of $\sim 23.19\%$ in the compressive property at room temperature. The alloy with a La/Nd ratio of 1/1 (S4) has a peak compression strength. The compressive property begins to decrease when the La/Nd ratio is greater than 1/1. As the La/Nd ratio increases from 0/0 to 3/2, the compressive property at high temperature increases from 283.98 MPa to the optimal ultimate compressive strength of 346.55 MPa and then decreases to 302.31 MPa. High-temperature compression strength and Vickers hardness reach the optimal ratio when the La/Nd ratio is 2/3 (S3). Adding REs reduces the content of $Mg_{17}Al_{12}$ in the alloy, which may slightly reduce the hardness and strength of the alloy. However, the formed Al_xRE_y ($Al_{11}RE_3$ and Al_2RE) can effectively improve the hardness and strength of the alloy, especially the high-temperature mechanical properties [27].

Figure 6 shows the engineering stress-strain curves of the squeeze-cast alloys. The difference in compression strain is somewhat significant for the squeeze-cast alloys at room temperature. The addition of REs increases strain, but the yield stage during compression becomes indistinct. The alloy with the most significant strain is the alloy with a La/Nd ratio of 2/3 (S3). Due to the large amount of coarse necklace-shaped $Mg_{17}Al_{12}$ distributed in the grain boundaries, AZ91 alloy has high strength and poor plasticity. Adding REs to the alloy greatly reduces the content of $Mg_{17}Al_{12}$ in the alloy, thereby improving the plasticity of the alloy. At high temperature, the difference in compressive strain is negligible compared with compression at room temperature. The reason may be that the $Mg_{17}Al_{12}$ in the alloy has been softened (this is also the main reason for the poor performance of AZ91 at high temperature [28]), so the plasticity of the alloy is less affected.

To verify the fracture mechanisms and their relations with REs of the alloys, the fracture surface and the EDS mapping analysis are presented in Figs. 7 and 8, respectively. It can be seen from the macro fracture photos of the squeeze-cast alloys shown in Fig. 6 that
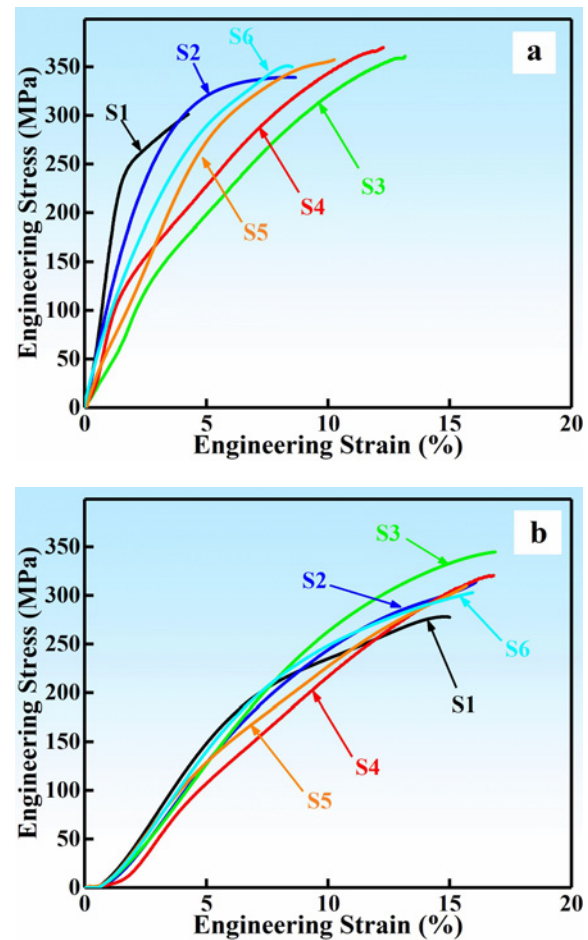
Fig. 6. Compression stress-strain curves of squeeze-cast alloys: S1–S6: (a) 293 K; (b) 423 K.

the fracture surfaces are approximately at a 45-degree angle to the axis. The microscopic characteristics of the fracture are mainly cleavage fracture. The fracture surface of the alloys without REs added showed a severely damaged state at both room temperature and high-temperature compression. The fracture surface of the alloy with REs added is less severe, and the fractography becomes smoother [21]. The EDS mapping result shown in Fig. 8 of the fracture surface
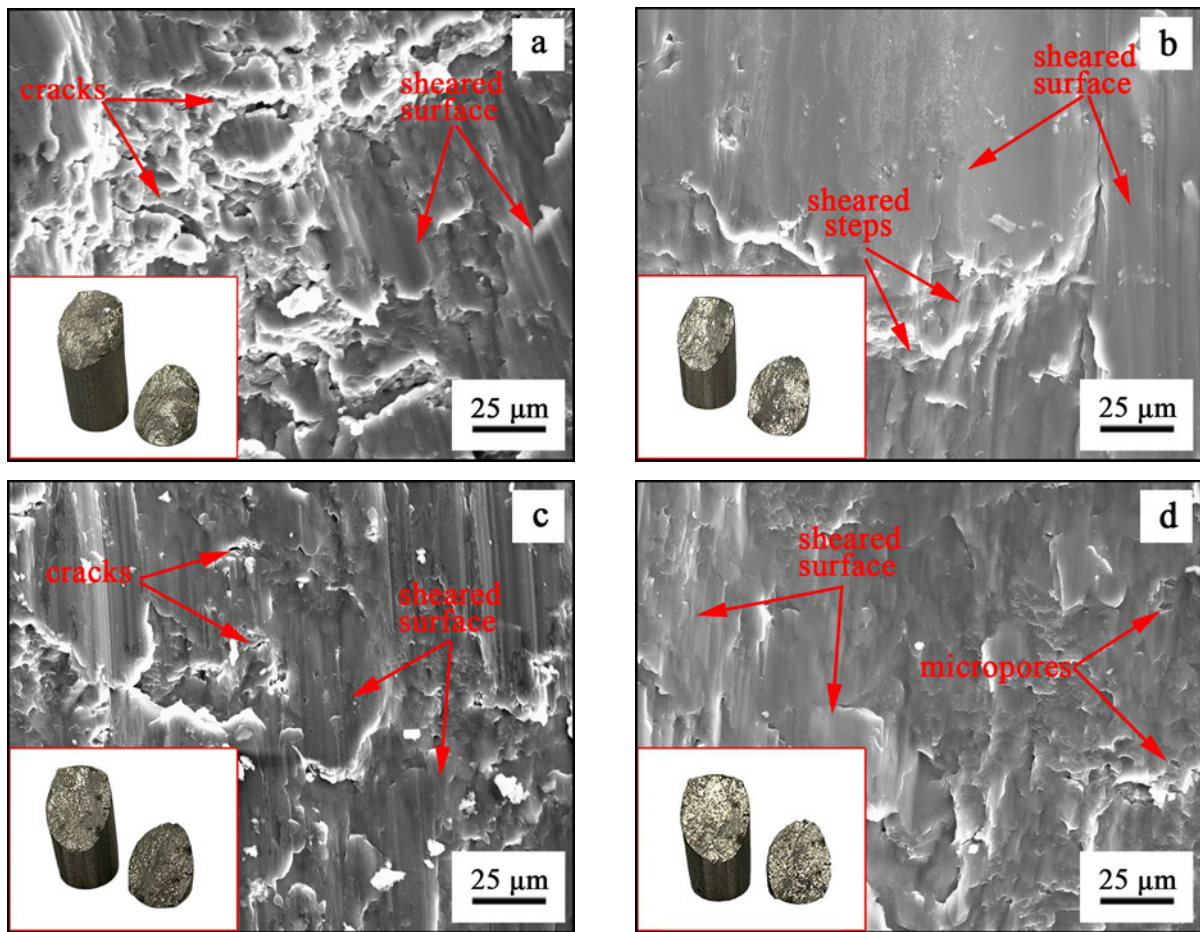
Fig. 7. Fracture morphologies of alloys: (a) Mg-Al-Zn alloy (293 K); (b) Mg-Al-Zn-La-Nd alloy (293 K); (c) Mg-Al-Zn alloy (423 K); (d) Mg-Al-Zn-La-Nd alloy (423 K).

reveals that Al, La, and Nd elements presenting aggregation morphology are visible near micropores and cleavage steps. Before the compressive stress reaches the critical ratio, the Al_xRE_y hinders the movement of grain boundaries and greatly improves the mechanical properties of the alloy. However, after the stress reaches the critical ratio, Al_xRE_y forms microvoids or microcracks at the Al_xRE_y/matrix interfaces and develops into the source of crack propagation. Zhang et al. [29] reported that the microcracks originate at the interface between Al_xRE_y and the matrix.

Powell et al. [8] reported that La segregated preferentially into needle-shaped $Al_{11}La_3$ phase while Nd partitioned into the granular Al_2Nd phase. They also reported that the formation of $Al_{11}RE_3$ and Al_2RE is sensitive to rare earth individuals. Meanwhile, the solubility of La is lower than that of Nd, and La would likely segregate around the grain boundaries. It is accessible that the second phase would increase as La/Nd ratio increases. Liu et al. [30] reported similar conclusions. Therefore, the La/Nd ratio may affect the content of needle-shaped $Al_{11}RE_3$ and granular Al_2RE in the Mg-Al-Zn-La-Nd alloy. Cui et al.

[31] reported that the length and quantity of acicular $Al_{11}RE_3$ phase would be quite different when dual REs with different La/Nd ratios are added to AZ91. However, for the granular Al_2RE it is difficult to achieve the statistical measurement measure due to its small volume and quantity. The EDS analysis results of the fracture surface in Fig. 8 indicate that the fracture of the Mg-Al-Zn-La-Nd alloy may be related to Al_xRE_y. The size, shape, number, and distribution of secondary phases affect the mechanical properties of the alloy [32]. $Al_{11}RE_3$, which is distributed in a large amount at the grain interiors and grain boundaries, is more likely to cause local stress concentration than Al_2RE and is also inclined to initiate a crack. In conclusion, adding dual REs with an appropriate La/Nd ratio to Mg-Al-Zn alloy can effectively improve its performance.

4. Conclusions

This study has designed and prepared six squeeze--cast Mg-Al-Zn-La-Nd alloys with different La/Nd
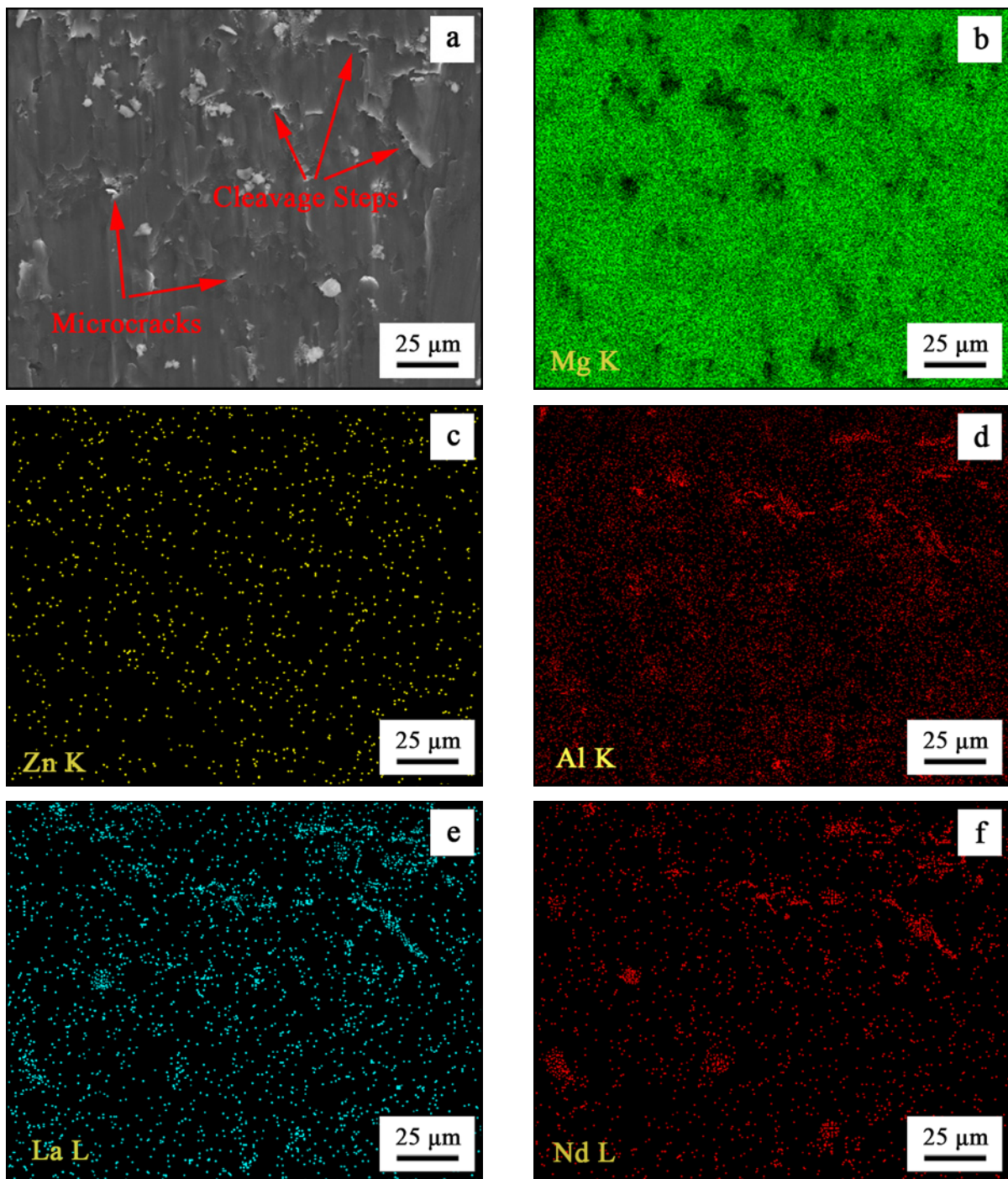
Fig. 8. The EDS mapping analysis of the fracture surface of Mg-Al-Zn-La-Nd alloy: (a) SEM image of Mg-Al-Zn-La-Nd alloy; (b) Mg K; (c) Zn K; (d) Al K; (e) La L; (f) Nd L.

values and two as-cast Mg-Al-Zn-La-Nd alloys. Microstructures and mechanical properties of squeeze-cast alloys have been discussed. The conclusions can be summarized as follows:

1. The grain size and the area friction of $Mg_{17}Al_{12}$ phase in squeeze-cast Mg-Al-Zn-La-Nd alloys change with increasing La/Nd value. As the La/Nd value increases from 0/0 to 3/2, the grain size decreases remarkably at first and then increases. When the La/Nd value is 2/3 and 1/1, the average grain size and $Mg_{17}Al_{12}$ area fraction of the alloy are minimum.

2. The XRD analysis results reveal that the La/Nd value significantly affects phase content, especially the change of phases at the scanning angle of 33.47° and 33.92°. With the increasing La/Nd value, the peak with scanning angles of 33.47° corresponding to (033)

plane reflection of $Al_{11}La_3$ increases, and the peak with the scanning angle of 33.92° corresponding to (130) plane reflection of $Al_{11}Nd_3$ decreases.

3. Both the Vickers hardness and the compression properties increase firstly and then decrease as the La/Nd value increases from 0/0 to 3/2. When the La/Nd value is 2/3, the Vickers hardness and high-temperature compressive property reach their peaks (82.15 HV and 346.55 MPa, respectively). The alloy with peak room temperature compressive property is the alloy with a La/Nd value of 1/1.

Acknowledgements

References

[1] A. Srinivasan, U. Pillai, B. Pai, Effect of Pb addition on aging behavior of AZ91 magnesium alloy, Mater. Sci. Eng. A 452 (2007) 87–92. doi:10.1016/j.msea.2006.10.119

[2] S. M. Zhu, M. Gibson, J. F. Nie, M. A. Easton, Microstructural analysis of the creep resistance of die-cast Mg-4Al-2RE alloy, Scripta Mater. 58 (2008) 477–480. doi:10.1016/j.scriptamat.2007.10.041

[3] B. Amir Esgandari, H. Mehrjoo, B. Nami, S. M. Miresmaeili, The effect of Ca and RE elements on the precipitation kinetics of Mg17Al12 phase during artificial aging of magnesium alloy AZ91, Mater. Sci. Eng. A 528 (2011) 5018–5024. doi:10.1016/j.msea.2011.03.022

[4] Q. Zhao, Y. Wu, W. Rong, K. Wang, Effect of applied pressure on microstructures of squeeze cast Mg-15Gd-1Zn-0.4Zr alloy, J. Magnes. Alloy 6 (2018) 197–204. doi:10.1016/j.jma.2018.04.001

[5] H. Zhou, X. Zeng, L. Liu, Y. Zhang, Effect of cerium on microstructures and mechanical properties of AZ61 wrought magnesium alloy, J. Mater. Sci. 39 (2004) 7061–7066. doi:10.1023/B:JMSC.0000047551.04037.fe

[6] L. Ke-Jie, L. Quan-An, J. Xiao-Tian, C. Jun, Effects of Sm addition on microstructure and mechanical properties of Mg-6Al-0.6Zn alloy, Scripta Mater. 60 (2009) 1101–1104. doi:10.1016/j.scriptamat.2009.02.048

[7] G. Pettersen, H. Westengen, R. Høier, O. Lohne, Microstructure of a pressure die cast magnesium – 4 wt.% aluminium alloy modified with rare earth additions, Mater. Sci. Eng. A 207 (1996) 115–120. doi:10.1016/0921-5093(95)10035-0

[8] B. R. Powell, V. Rezhets, M. P. Balogh, R. A. Waldo, Microstructure and creep behavior in AE42 magnesium die-casting alloy, JOM 54 (2002) 34–38. doi:10.1007/BF02711864

[9] H. Zou, X. Zeng, C. Zhai, W. Ding, Effects of Nd on the microstructure of ZA52 alloy, Mater. Sci. Eng. A 392 (2005) 229–234. doi:10.1016/j.msea.2004.09.010

[10] J. Zhang, K. Liu, D. Fang, X. Qiu, Microstructure, tensile properties, and creep behavior of high-pressure die-cast Mg-4Al-4RE-0.4 Mn (RE = La, Ce) alloys, J. Mater. Sci. 44 (2009) 2046–2054. doi:10.1007/s10853-009-3283-4

[11] I. J. Polmear, Magnesium alloys and applications, Mater. Sci. Tech. 10 (1994) 1–16. doi:10.1179/mst.1994.10.1.1

[12] Y. Lü, Q. Wang, X. Zeng, W. Ding, Effects of rare earth on the microstructure, properties and fracture behavior of Mg-Al alloys, Mater. Sci. Eng. A 278 (2000) 66–76. doi:10.1016/S0921-5093(99)00604-8

[13] H. Bayani, E. Saebnoori, Effect of rare earth elements addition on thermal fatigue behaviors of AZ91 magnesium alloy, J. Rare Earth. 27 (2009) 255–258. doi:10.1016/S1002-0721(08)60230-6

[14] M. R. Ghomashchi, A. Vikhrov, Squeeze casting: An overview, J. Mater. Process. Tech. 101 (2000) 1–9. doi:10.1016/S0924-0136(99)00291-5

[15] J. Majhi, A. Mondal, Microstructure and impression creep characteristics of squeeze-cast AZ91 magnesium alloy containing Ca and/or Bi, Mater. Sci. Eng. A 744 (2019) 691–703. doi:10.1016/j.msea.2018.12.067

[16] S. Lee, S. H. Lee, D. H. Kim, Effect of Y, Sr, and Nd additions on the microstructure and microfracture mechanism of squeeze-cast AZ91-X magnesium alloys, Metall. Mater. Trans. A 29 (1998) 1221–1235. doi:10.1007/s11661-998-0249-0

[17] Y. Zhang, G. Wu, W. Liu, L. Zhang, Effects of processing parameters and Ca content on microstructure and mechanical properties of squeeze casting AZ91-Ca alloys, Mater. Sci. Eng. A 595 (2014) 109–117. doi:10.1016/j.msea.2013.12.014

[18] G.-D. Tong, H.-F. Liu, Y.-H. Liu, Effect of rare earth additions on microstructure and mechanical properties of AZ91 magnesium alloys, T. Nonferr. Metal. Soc. 20 (2010) s336–s340. doi:10.1016/S1003-6326(10)60493-1

[19] M. Sun, X. Hu, L. Peng, P. Fu, Effects of Sm on the grain refinement, microstructures and mechanical properties of AZ31 magnesium alloy, Mater. Sci. Eng. A 620 (2015) 89–96. doi:10.1016/j.msea.2014.09.106

[20] J. Zhang, M. Zhang, J. Meng, R. Wu, Microstructures and mechanical properties of heat-resistant high-pressure die-cast Mg-4Al-xLa-0.3Mn (x = 1, 2, 4, 6) alloys, Mater. Sci. Eng. A 527 (2010) 2527–2537. doi:10.1016/j.msea.2009.12.048

[21] Y.-X. Wang, J.-W. Fu, Y.-S. Yang, Effect of Nd addition on microstructures and mechanical properties of AZ80 magnesium alloys, T. Nonferr. Metal. Soc. 22 (2012) 1322–1328. doi:10.1016/S1003-6326(11)61321-6

[22] M. Su, J. Zhang, Y. Feng, Y. Bai, Al-Nd intermetallic phase stability and its effects on mechanical properties and corrosion resistance of HPDC Mg-4Al-4Nd-0.2 Mn alloy, J. Alloy. Compd. 691 (2017) 634–643. doi:10.1016/j.jallcom.2016.08.310

[23] J. Wang, L. Wang, J. An, Y. Liu, Microstructure and elevated temperature properties of die-cast AZ91-xNd magnesium alloys, J. Mater. Eng. Perform. 17 (2008) 725–729. doi:10.1007/s11665-007-9168-2

[24] A. R. Miedema, P. F. De Châtel, F. R. De Boer, Cohesion in alloys – fundamentals of a semi-empirical model, Physica B+C 100 (1980) 1–28. doi:10.1016/0378-4363(80)90054-6

[25] A. K. Niessen, F. R. De Boer, R. Boom, P. F. De Châtel, Model predictions for the enthalpy of formation of transition metal alloys II, Calphad 7 (1983) 51–70. doi:10.1016/0364-5916(83)90030-5

[26] H. Yu, Y. Xin, M. Wang, Q. Liu, Hall-Petch relationship in Mg alloys: A review, J. Mater. Sci. Technol. 34 (2018) 248–256. doi:10.1016/j.jmst.2017.07.022

[27] G. Wu, C. Wang, M. Sun, W. Ding, Recent developments and applications on high-performance cast magnesium rare-earth alloys, J. Magnes. Alloy. 9 (2021) 1–20. doi:10.1016/j.jma.2020.06.021

[28] S. Ganguly, S. T. Reddy, J. Majhi, P. Nasker, Enhancing mechanical properties of squeeze-cast AZ91 magnesium alloy by combined additions of Sb and SiC nanoparticles, Mater. Sci. Eng. A (2021) 140341. doi:10.1016/j.msea.2020.140341

[29] J. Zhang, J. Wang, X. Qiu, D. Zhang, Effect of Nd on the microstructure, mechanical properties and corrosion behavior of die-cast Mg-4Al-based alloy, J. Alloy. Compd. 464 (2008) 556–564. doi:10.1016/j.jallcom.2007.10.056

[30] X. Liu, Z. Zhang, Q. Le, L. Bao, Effects of Nd/Gd value on the microstructures and mechanical properties of Mg-Gd-Y-Nd-Zr alloys, J. Magnes. Alloy. 4 (2016) 214–219. doi:10.1016/j.jma.2016.06.002

[31] P. Cui, M. Hu, Z. Ji, H. Xu, Effect of La/Nd ratio on microstructure and mechanical properties of as-cast AZ91-xLa/Nd alloy, Mater. Res. Express 7 (2020) 026531. doi:10.1088/2053-1591/ab7162

[32] J. Zhang, D. Zhang, Z. Tian, J. Wang, Microstructures, tensile properties and corrosion behavior of die-cast Mg-4Al-based alloys containing La and/or Ce, Mater. Sci. Eng. A 489 (2008) 113–119. doi:10.1016/j.msea.2007.12.024